



Performance assessment of vegetable oil–based MQL in milling of additively manufactured AlSi10Mg for sustainable production

Nimel Sworna Ross¹ · M. Belsam Jeba Ananth² · J. M. Jafferson³ · L. Rajeshkumar⁴ · M. Saravana Kumar⁵

Received: 31 March 2022 / Revised: 8 June 2022 / Accepted: 15 June 2022 / Published online: 1 July 2022
© The Author(s), under exclusive licence to Springer-Verlag GmbH Germany, part of Springer Nature 2022

Abstract

The precision of lightweight components produced during machining of aluminium alloy is critical as a reason of its high chemical reactivity to the tool metal when cutting. Mineral-based cutting fluids (CFs) used in the manufacturing industry pollute the environment and offer adequate health risks to the operators; it is vital to develop environmentally friendly machining technologies. As a corollary, vegetable oil (VO) must be used to replace mineral oil to avoid pollution. In recent decades, VO produced from raw edible sources is a reliable source for greener CF. Toxic fumes and skin irritations caused by conventional CFs are all avoided when using VO in machining. In this research, an additively manufactured AlSi10Mg specimen was machined with distinct coolants to enhance the surface trait. The mechanical performance such as tensile, hardness and wear strength were investigated to prove that the 90° oriented AlSi10Mg parts show better strength. Further, the machining of 90° oriented AlSi10Mg parts was performed to examine certain issues such as surface morphology, flank wear and cutting temperature using different cooling regimes (flood and MQL with soybean oil). As a result of heat generation in the cutting zone, the surface deteriorates and the cutter needs to be replaced often. The MQL with VO minimises the heat generated at the cutting region and lessened the roughness to 25–42% and temperature to 24–39% with flood coolant. Additionally, the microstructure under MQL cutting produced fine grains. The desirability function was employed to find the ideal cutting condition for sustainable manufacturing.

Keywords Additive manufacturing · LPBF · AlSi10Mg · MQL · Optimization

✉ M. Saravana Kumar
saravana312@gmail.com; mskumar@nitt.edu

Nimel Sworna Ross
nimelross@gmail.com

M. Belsam Jeba Ananth
belsama@srmist.edu.in

J. M. Jafferson
jafferson.jm@vit.ac.in

¹ Department of Mechanical Engineering, Saveetha School of Engineering, SIMATS, Chennai 602105, Tamil Nadu, India

² Department of Mechatronics Engineering, SRM Institute of Science and Technology, Kattankulathur, Tamil Nadu, India

³ CoE for Additive Manufacturing, VIT University, Chennai Campus, Chennai, India

⁴ Department of Mechanical Engineering, KPR Institute of Engineering and Technology, Coimbatore 641407, Tamilnadu, India

⁵ Department of Production Engineering, National Institute of Technology, Tiruchirappalli, Tamil Nadu, India

1 Introduction

The current recognised direction and emerging trend in manufacturing techniques are aimed at meeting the demands for shape precision, as well as surface quality [1]. Metal printing is an additive manufacturing (AM) technology that is now gaining traction in a variety of industries, including energy, aerospace, automotive, marine and healthcare. Metal AM is characterised by many advantages such as equipment repeatability for various products and a shorter lead time of production [2, 3]. This technology might readily manufacture tailorable components for nuclear power plants, medical implants that are custom-made for each patient, and a few more personalised parts [4, 5]. This technology enables many-in-one product integration, resulting in a significant return on investment, as well as the preservation of product inheritance for which supply networks are no longer necessary [6]. Amongst modern AM technologies, the laser powder bed fusion (LPBF) family has expanded a lot of interest because of the ultrafine microstructures that occur and the

accompanying improved mechanical properties [7]. Components in LPBF are created from a powdery raw material through the specified layer-by-layer combination of distinct volume elements. This manufacturing method opens up new options for the user in terms of design flexibility, the production of highly customised parts and the customization of products to the needs of specific applications [8].

The LPBF process has been extensively studied when used to grades of steel, nickel-chrome alloys and titanium alloys. Aluminium (Al) alloys have also been the subject of research. Al and its alloys do undoubtedly have considerable future potential, owing to their low density, which can result in massive volume savings [9]. Because of the outstanding mechanical characteristics and process accomplishment, AlSi10Mg appears to be a better fit for selective laser melting (SLM) technology than the other Al alloys [10]. Various research on the structure and characteristics of AlSi10Mg prepared by SLM have also been available [11]. It is a near eutectic alloy of aluminium with a composition of 12.6% by wt. of silicon, 90% by wt. of aluminium and magnesium of 0.5% by wt. [12, 13]. This alloy is mostly subjected to LPBF manufacturing owing to its eutectic composition, allowing the manufactured components to have a greater volumetric density and the creation of a final product free of solidification cracking [14]. Meanwhile, the yield stress of 250–300 MPa, a tensile stress of around 400 MPa and a strain rate of around 7% could be achieved, according to recent studies, when AlSi10Mg alloy was manufactured by the LPBF process. Such higher strength could be possibly due to the finer sub-grain cellular structures which results from the LPBF method [15, 16]. Different factors are responsible for mechanical characteristics, surface finish and accuracy of LPBF manufactured components. Amongst these, laser power, scanning speed, LT, scanning technique and part orientation are the important process parameters for making the product [17]. The dimensional precision and surface quality of components produced with the LPBF technique are frequently inadequate, necessitating further processing [18]. When it comes to improving the surface quality of the LPBF components, it is important to use subtractive machining techniques such as turning and milling as well as grinding and polishing [19]. The nominal roughness of the as-printed LPBF components ranged between 3 and 40 μm while the error range pertaining to dimensional accuracy lay between 0.01 and 3.4% [20].

Metal cutting is one of the most used approaches for shaping a product or component in the manufacturing industry to achieve the desired product [21, 22]. Zimmermann et al. [23] examined the impact of LPBF on the machinability of AM-AlSi10Mg while milling in regard to chip formation, surface morphology, microhardness

and formation of burr concerning production parameter settings for the end mill's feed motion. The LPBF material shows severe flakes emerging from the surface when machining without any coolant. Dabwan et al. [24] examined the LPBF produced SS 316 subjected to milling for analysing the influence of part orientations over the final characteristics of the material. Four-layer thickness values such as 30, 60, 80 and 100 μm were adopted to fabricate LPBF components and they were subjected to the milling process to analyse the influence of LT. From the results, it was stated by the authors that part orientation had the least influence during the milling of LPBF parts while the components with an LT of 60 μm exhibited better surface integrity when compared with their other counterparts. When compared to cast or wrought alloys, LPBF components have a different machinability character; the quality of the machined surface of an LPBF component has yet to be studied for improvement [25]. Machining of LPBF components must be done in a disparate cooling medium to achieve this. Amongst various methods, flood cooling methods offer a lower heat generation at the interface of the cutter and workpiece [26]. However, from an environmental standpoint, the coolants used in flood cooling technologies are dangerous and toxic to the environment, and their disposal costs a lot of money. Disposal of cutting fluids (CFs) is estimated to account for roughly 16% of the whole product cost, which must be addressed [27, 28]. According to the International Agency for Research on Cancer, CFs generated from petroleum products with polyaromatic and heterocyclic rings are more hazardous to the environment, and their interaction with the skin causes a variety of skin illnesses. The usage of CFs must be optimised to avoid such environmental, medical and economic consequences [29]. When performing machining and metal-cutting operations, some researchers have switched to minimal quantity lubrication (MQL) in place of flood cutting. To improve heat transfer and tribological features during milling, MQL uses high-velocity coolant droplets that are injected into the tool-workpiece interface [21, 30].

Nevertheless, there is very little information recorded on the lubricating properties of distinct cooling methods while machining LPBF produced AlSi10Mg. A literature scarcity was also noticed which had not addressed the effects of LPBF process parameters on the machinability. In light of all of the above, current research focuses on the production of 90° oriented AlSi10Mg parts using the LPBF process and its mechanical performance was investigated to state that the 90° oriented AlSi10Mg possesses improved strength and then it is subjected to milling trials with varied speed-feed combo and environment. Upon the optimization of the milling process parameters, ideal surface roughness, flank wear and milling temperature could be obtained as a response.

2 Materials and methods

2.1 LPBF process

The workpiece AlSi10Mg was manufactured by the LPBF technique (Model: EOS-M290) at an orientation of 90°. LPBF machine inherently contains a building platform with a dimension of 250 × 250 × 325 mm. The printing chamber was operated with 400-W laser power in an inert Argon atmosphere and with a focus diameter of 100 µm. The workpiece was fabricated with a LT of 30 µm at 1300 mm/s scanning speed. If the LT was increased, the exposure time of the printed material to the laser reduces which in turn converts the process into an economic one. A carrying unit containing AlSi10Mg alloy powder (particle size of around 16–20 µm) was placed to dispense the metal powder continuously during the entire workpiece printing process. A strong build platform was made available along with the dispenser unit for providing space to the printed specimens until the completion of the printing process. The density of the printed specimens was measured using Archimedes' principle and was found to be 99 ± 0.01%. Table 1 enlists

the chemical constituents of AM-AlSi10Mg alloy. The elemental mapping (Fig. 1) on the face of the LPBF produced AlSi10Mg proved the presence of main constituents Al, Si and Mg. As-built LPBF materials were subjected to machining without heat treating them to assess the original machinability.

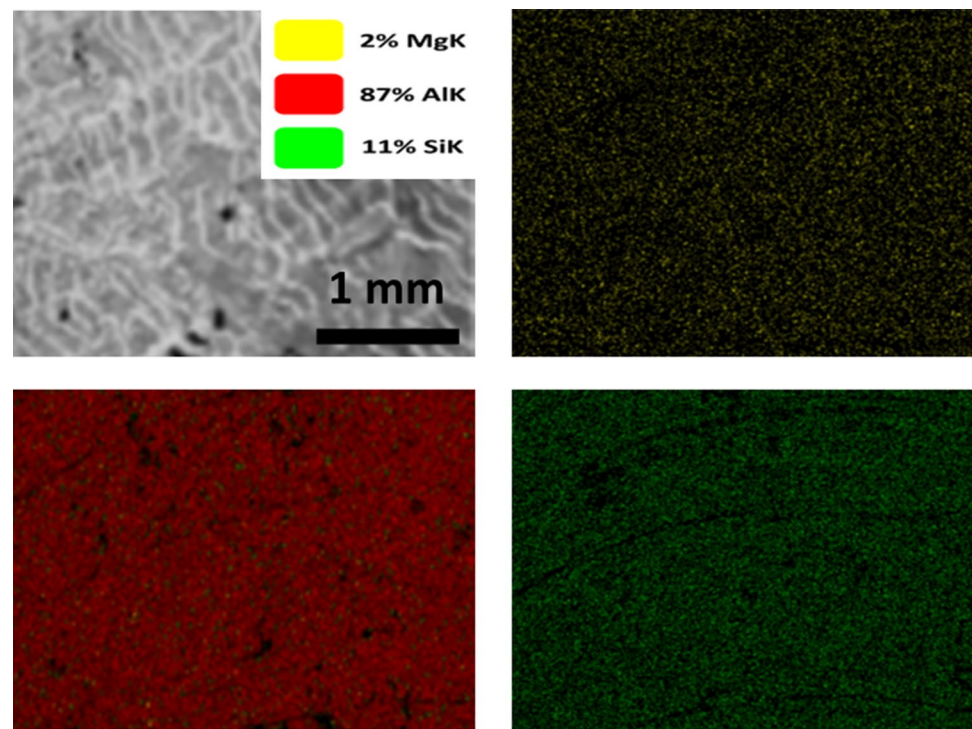
2.2 Machining performance

Milling operations were performed in a vertical milling centre (Model: Avia-VMC 800) using an end mill cutter of 6 mm diameter (PVD-TiAlN coated). The milling cutter comprises of 18-mm flute length with four flutes in it. The surface of LPBF printed alloys were machined to investigate the machinability of AM-AlSi10Mg; the milling operation was carried out in a direction perpendicular to the build direction. The hardness of the LPBF alloy was measured to be 113 HV. Experimental trials were carried out with 2 levels of machining environments (flood and MQL condition), 2 levels of feed rate (*f*) (0.1 and 0.12 mm/rev) and 4 levels of cutting speed (*V_c*) (1200–2400 rpm at 400-rpm intervals) to assess the surface quality. The input conditions for cutting were selected based on the previous research and the tool

Table 1 Chemical elements of AlSi10Mg (wt%)

Material	Si	Mg	Fe	Cu	Mn	Others	Al
AlSi10Mg	9.0–11.0	0.40–0.60	≤2.0	≤0.60	≤0.35	≤0.25	Bal

Fig. 1 EDS elemental mapping of LPBF produced AlSi10Mg



maker's preferences [31]. Furthermore, sufficient trials were conducted to finalise the input parameters. Figure 2 shows the manufacturing and measuring instruments. Oil–water emulsion at a ratio of 1:20 was used as a coolant during flood machining conditions, and it was applied at a mass flow rate of 2.5 L/min directly onto the interface of the tool and workpiece. MQL setup was an in-house-built setup and it comprises of a pneumatic pump that sucks the soybean oil of absolute viscosity 0.0391 Pa from a 5 L reservoir. Atomized VO was sprayed onto the interface of the tool and workpiece at 3-bar pressure and a mass flow rate of 1 ml/min. Distance between the tool-workpiece interface and MQL nozzle was kept at 30 mm and the angle was maintained as 45° to the feed direction. The experimental methodology is presented in Fig. 2.

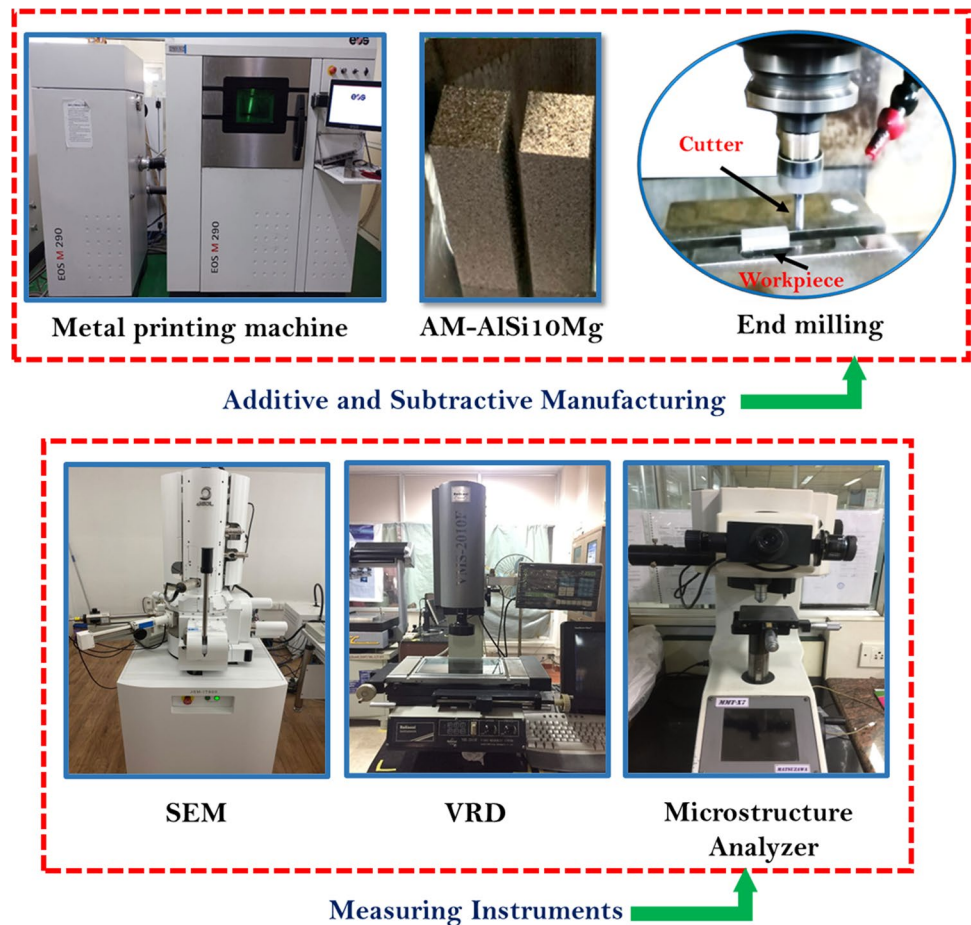
2.3 Measurement of mechanical and machining performance

The mechanical properties such as tensile, hardness and wear strength were evaluated on the fabricated 90° oriented AlSi10Mg parts. Universal Testing Machine (H50KL, Tinius Olsen Computerized model) was used to analyse the yield strength,

elongation percentage, reduction in area percentage and the tensile strength for the AlSi10Mg parts. Similarly, Brinell macro-hardness tester (HR-320, Mitu Toyo South Asia Pvt. Ltd.) was adopted to predict the hardness of the as-built AlSi10Mg parts based on ASTM E10 standard. Pin-on-disc wear testing apparatus was used to find out the wear resistance of the fabricated 90° oriented AlSi10Mg parts. The trials were conducted on the dry sliding condition according to the ASTM G-99 standard.

Under different combinations of speed-feed and machining environments, the milling operation was performed for a length of 30 mm during each trial. The surface roughness of the freshly milled surface was examined for its surface roughness value using the SE model surface roughness tester. Three different values of surface roughness were measured at a length of 0.8 mm at distinct places and the average value was taken for the analysis. The cutting temperature at the interface of the tool and workpiece was recorded using an infrared thermometer (Model: HTC-IR Thermometer) with a temperature range of – 50 to 500 °C. A video recording device (VRD)-Model: 2010-F was used to record the flank wear at the milling cutter side. Flank wear morphology and the surface defects were visualised through a scanning electron microscope (SEM) of JEOL make.

Fig. 2 Experimental methodology



3 Results and discussion

3.1 Mechanical characterisation

3.1.1 Tensile test

The tensile specimen was fabricated based on the ASTM E8 standard. The fabricated specimen was subjected to the tensile load in Universal Testing Machine (H50KL, Tinius Olsen Computerized model) and evaluated the tensile properties such as ultimate tensile strength (UTS), yield strength (YS), percentage of elongation and reduction area of the 90° oriented AlSi10Mg parts. From the results, it was evident that the 90° oriented parts show maximum UTS of 418 MPa. This result shows good agreement with Kumar et al. [6]. This significant improvement in the tensile strength of the fabricated 90° oriented parts was mainly due to the building direction of the fused particles. The direction of the tensile load was perpendicular to the direction of the sintered particles [32]. At the time of application of load, the presence of a strong bond between the α -aluminium and the eutectic Si particles resists the dislocation moments which leads to the enhanced tensile strength [33, 34]. So, the maximum yield strength of 234 MPa was observed in the 90° oriented parts. Due to the presence of ductile behaviour of aluminium, the fabricated 90° oriented parts possess a certain elongation % of 5.46 which attributes to the reduction in area % of 6.27. The presence of eutectic Si particles increases the brittle nature of the fabricated parts. So, this was the reason behind the presence of combined ductile and brittle behaviour in the fractured parts. The fractography of the fractured surface was analysed with the help of SEM. The propagation of cracks originates at the stress concentrated region at the interface of the eutectic Si particles. Multiple macro cracks were evident in the fabricated 90° oriented parts after the tensile test. It was noted the propagation of cracks follows the direction of the sintering of the particles [35]. This was due to the weaker bonding between adjacent layers of the fused particles which attribute towards the transgranular facets. The presence of dimple and necking represents the ductile behaviour of aluminium (Fig. 3). Similarly, the presence of cleavage facets was due to the brittle behaviour of eutectic Si particles. The presence of multiple microvoids was observed in the fractured surface which was formed during the melt pool solidification. During solidification, the presence of eutectic silicon particles creates high nucleation sites which attribute to the formation of the micropores. These micropores create a space that helps to the attainment of high strength of materials. Similarly, the occurrence of a high concentration of eutectic Si particles also enhances the high strength-to-weight ratio.

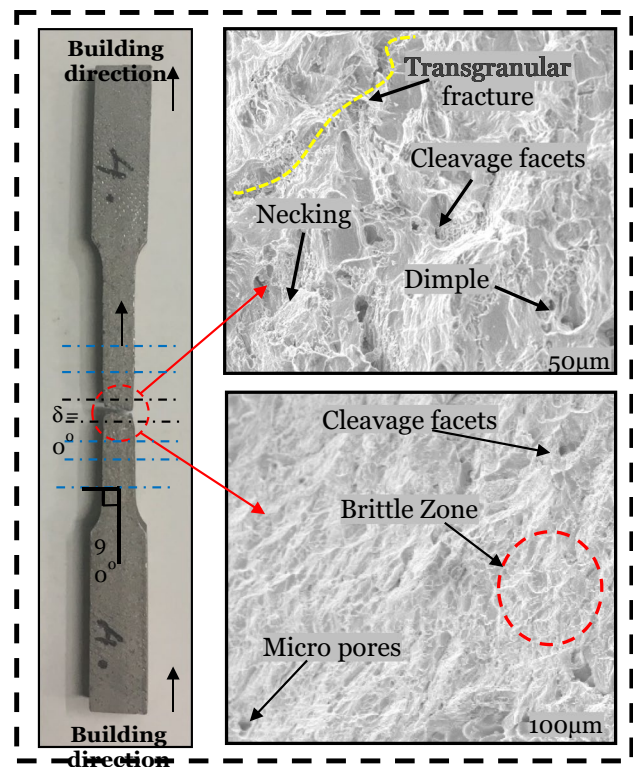


Fig. 3 Fractography of the fractured tensile specimen

3.1.2 Hardness test

The fabricated 90° oriented parts were carried out for Brinell macro-hardness test (HR-320, Mitu Toyo South Asia Pvt. Ltd.). The maximum hardness value of 107 HBW was observed in the fabricated 90° oriented parts. This maximum hardness value was due to the presence of strong bonding between the Al–Si particles, and also the fusion of consecutive layers makes the parts resist the indentation effect. The presence of Si particles shows high resistance to the indentation effect [36]. Multiple hardness values were taken at the various regions of the fabricated parts and the average value was drawn. It was observed that the maximum hardness value was obtained at the fused region where there was a strong bonding of Al–Si particles and the minimum hardness values were obtained between the fused layers.

3.1.3 Wear test

From the wear rate evaluation of the fabricated 90° oriented parts, the wear rate of $3.2 \times 10^{-4} \text{ mm}^3 \text{ N}^{-1} \text{ m}^{-1}$ was observed which was a lower wear rate when compared with the other literature. These wear analysis experiments were carried out with a constant load of 25 N, sliding

speed of 300 rpm and sliding distance of 1250 m. In the 90° oriented parts, the sliding direction was parallel to the direction of the fusion of the particles which was considered one of the major reasons for assisting high resistance to wear. The matting of the wear specimen with the counter disc creates a new layer. This layer prevents the formation of more wear debris and also resists wear rate [37]. It was noted that the wear debris formed during sliding action will act as the second body abrasive material and also the formation of the wear debris attributes to the ploughing action [38] and also delamination takes place due to high friction between the wear specimen and the abrasive counter disc which is shown in Fig. 4.

From the literature survey, it was revealed that the 90° oriented parts possess considerable improvement in mechanical properties when compared with the other-oriented parts [6]. In this research, the results obtained from the mechanical characterisation of 90° oriented parts show very good agreement with the previous research works.

3.2 Machinability of AM-AISI10Mg

3.2.1 Impact of surface roughness

Average surface roughness (R_a) was evaluated in this study to define the surface trait of the machined faces since it is considered to be the most suitable method by almost every manufacturing industry [39, 40]. Figure 5 illustrates the R_a measurements of milled faces at various V_c under flood and MQL environments, and it can be demonstrated that R_a falls as V_c climbs. This action is caused by a rise in C_T with a rise in V_c , which promotes thermal softening of the workpiece and greater elimination of worn surfaces, leading to lower R_a . At a V_c of 1200 rpm and a f of 0.12 mm/rev, the R_a measurement for MQL cutting is 0.725 μm and for flood cooling is 0.975 μm . R_a was improved by 25.62% in MQL cutting compared to flood cooling. When the V_c was 2400 rpm and for the same f mentioned above, the measurements received were 0.731 μm and 0.423 μm for MQL and flood

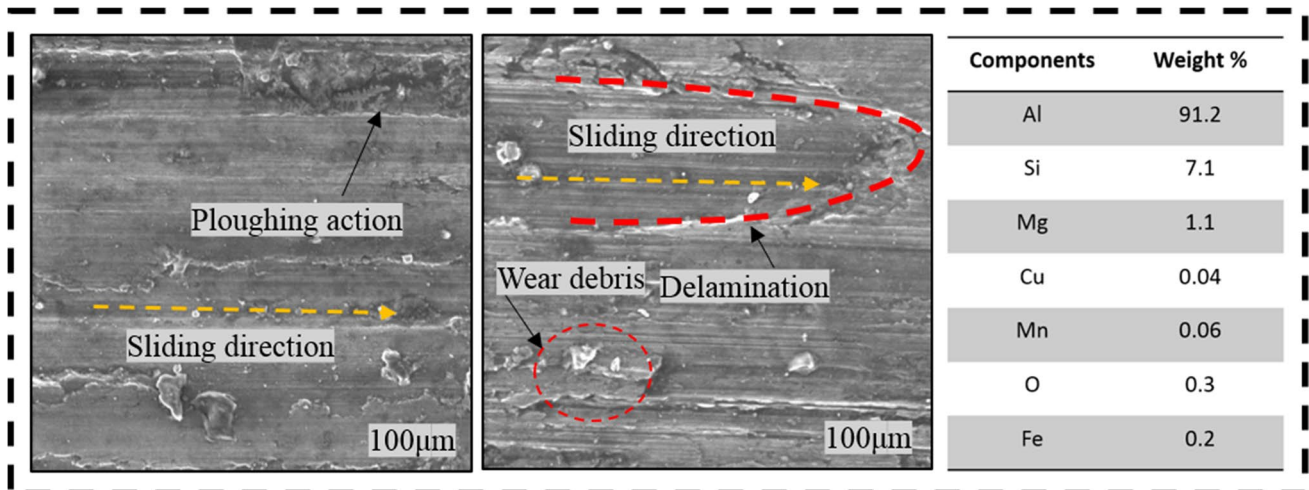
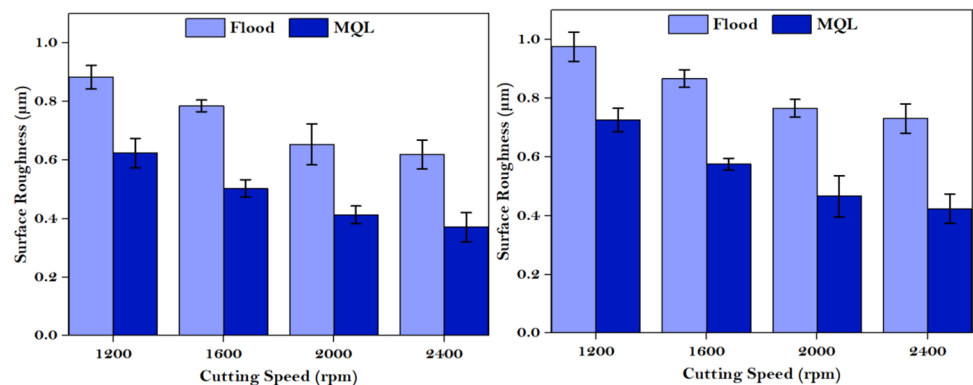


Fig. 4 Worn-out surface of the wear specimen

Fig. 5 Influence of cooling strategies on Roughness under distinct environments. **a** $f=0.10$ mm/rev and **b** $f=0.12$ mm/rev



cutting, respectively. MQL shows superiority (42.05%) over flood cooling. The use of MQL overall declines the Ra 25–42% concerning flood cooling. The reduction is achieved by spraying oil mist at a 45° angle on the rake face. The C_T at the cutting region is decreased by the supply of oil + air, resulting in fewer tool marks on the machined face, which lowers the Ra. Poor cooling effect by flood condition is the reason for higher Ra. Adhesion is crucial in deciding the quality of the machined face. When the glued material turned uncertain, it would have separated from that of the tool and stuck to the work surface, raising the machined surface's Ra [41]. Figure 6 shows the main effects plot for Ra. From the figure, it could be seen that the Ra was highly influenced by the environment followed by the Vc and f .

Figure 7 displays the 2D surface profiles of machined AlSi10Mg under varied cutting environments. It is seen evidently that the peaks formed are uneven and the deviation is more from the centerline, with the flood environment. But, under the MQL environment, the deviation is lesser concerning the centerline. The hard Si particles in the workpiece are the reason for more deviations. When it comes to MQL, better lubricity given by the VO curtails the cutter wear and paves the way for less deviation.

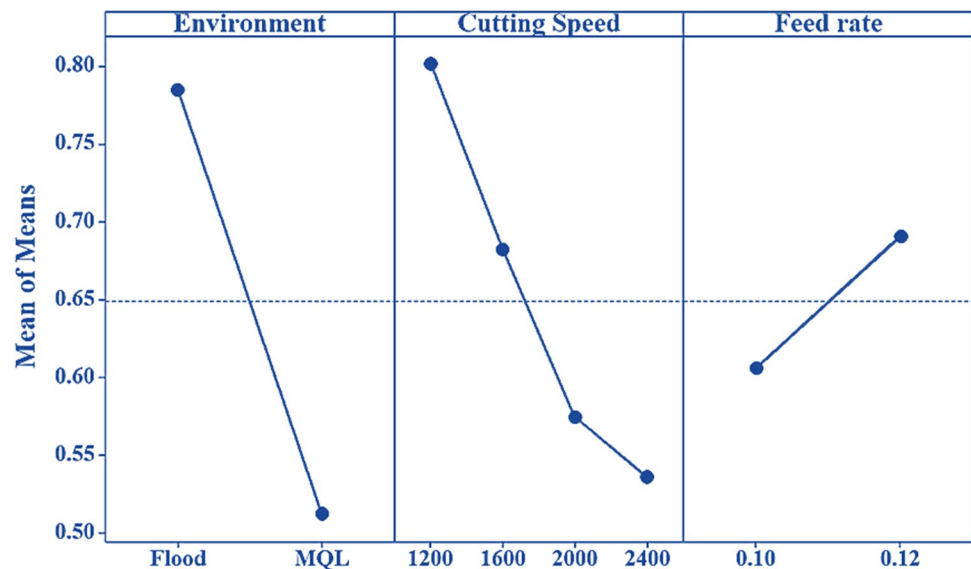
Figure 8 shows SEM pictures of milled surfaces on the left side. Under different environmental conditions, the surface structure of milled workpieces differs. Under flood condition, the surfaces of milled LPBF workpieces have a severe flaky structure. During tool engagement, the surface shows the roughness peak caused by linear feed and concomitant rotational motion through the material. The bigger the Ra, lower the rpm. Depending on the imperfections, the roughness will be increased. Machined AlSi10Mg debris were superficially present on the milled LPBF specimens [23].

This debris is most likely the flakes of AlSi10Mg that have been fully peeled away from the surface. Fewer flakes were seen when machined with MQL condition. The lube characteristic of oil mist is the reason for the good surface trait in contrast with flood cooling. 3D plots (right side) show highs and lows under both conditions. Comparatively, the MQL strategy shows fewer highs concerning flood cooling, which proves that the MQL technique lessened the friction at the cutting place effectively.

3.2.2 Impact of temperature

Figure 9 illustrates the C_T corresponding to flood and MQL environments. During metal cutting, the temperature became extreme at the chip–tool juncture. The noted C_T at 2400-rpm speed, 0.12-mm/rev feed and 1-mm depth of cut was 133.12 and 95.01 °C for flood and MQL conditions, respectively. It was noticed that 28.6% of C_T was reduced during MQL machining when compared with flood machining condition. In the case of MQL, the flow of compressed air enhances the efficiency of heat transfer amid cutting system and machining environment. Meanwhile, the oil film formed by the mist permeating into the chip–tool juncture reduced friction and there was the less build-up of heat [42]. However, the cooling ability depends only on the flow of air. Hence, the application of MQL resulted in a lower C_T concerning the flood environment. The MQL method contributes more than one effect while cutting the material explained by Yildirim et al. [40]. Firstly, the lubrication in MQL wraps the cutting region with a layer of oil and this helps to reduce friction. Secondly, MQL contributes to heat transfer due to the evaporation of droplets. The main effect plot for C_T is displayed in Fig. 10. Similar to Ra, the temperature at the cutting area is

Fig. 6 Main effects plot for surface roughness



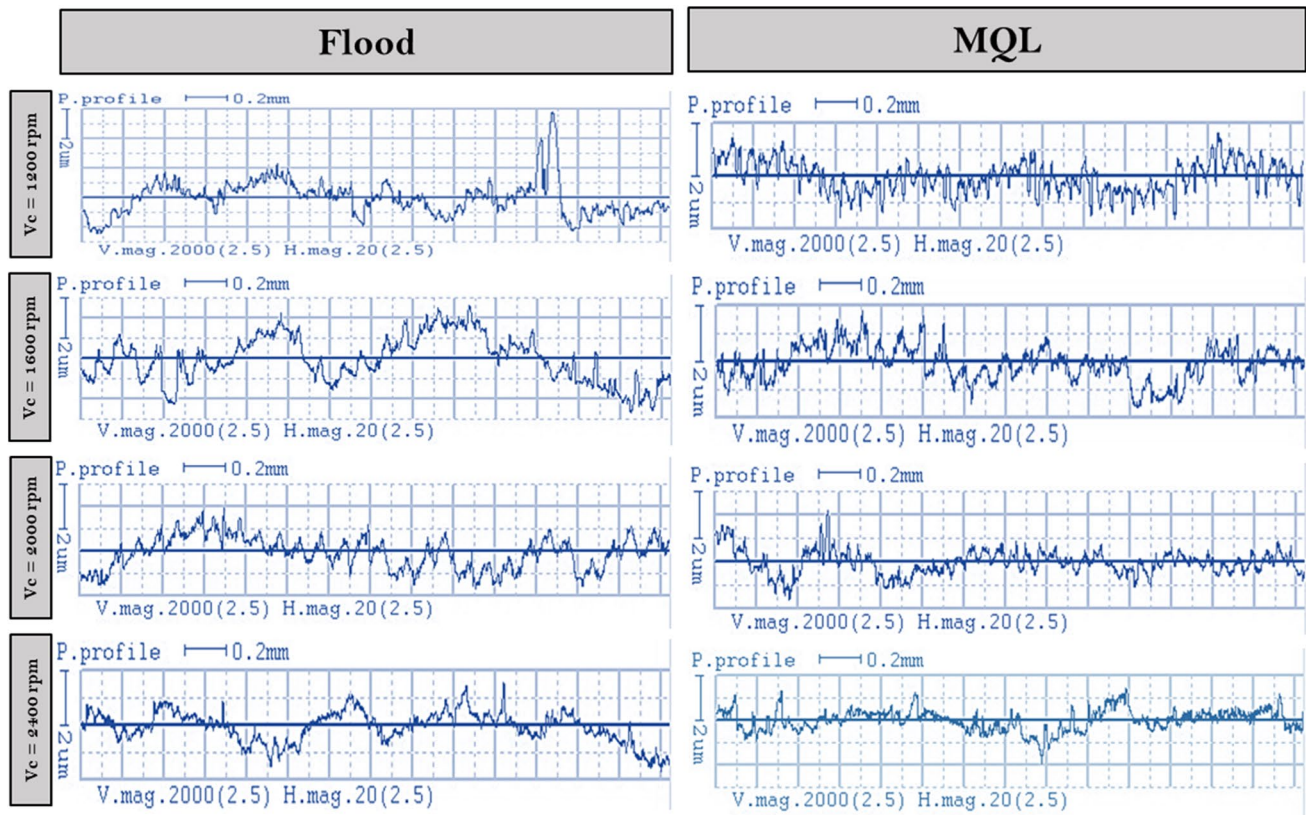


Fig. 7 2D roughness profiles under distinct environments at a $f=0.12$ mm/rev

also maximum influenced by the cutting environment. The higher cutting performance was obtained at MQL condition accounting for the higher efficiency of heat transfer [43].

3.2.3 Impact of flank wear

Figure 11 demonstrates how V_b varies depending on the environment (flood and MQL). The decline in friction at the tooltip was proportional to the change in V_b under various cutting strategies [44]. The increase in tool life is seen as the cutting temperature decreases. Due to cutter wear, the chip-tool contact increases, which causes an increase in machining force.

In shortage of lubrication and cooling during flood cutting, significant wear was created at the insert as a reason of frictional force and heat, which primes to shortest tool life. The highest V_b observed under flood cutting was 0.087 mm and the lowest was with MQL, which was 0.045 mm. The V_b was improved by 22.05% and 18.39% in MQL cutting associated with flood cooling at a V_c of 1200 and 2400 rpm. The use of MQL diminishes the V_b 18–31% related to flood condition. The outcome was associated with the nozzle position, the amount of oil used, the

spray device's pressure and even the capillarity impact on the cut surface. Figure 12 shows the main effects plot for V_b . The cutter wear was influenced by the environment to the maximum level. In MQL, the lubrication effect of the oil reduced the wear rate and, thus, implied an increased tool life when compared with flood cutting [45]. The oil droplets impacted the heat transfer and lubrication. The lubrication effect was more effective in relieving tool wear than simply providing a cooling medium.

The input variables have a major impact on the wear levels during the metal cutting process. The higher cutting parameters cause the cutting tool to encounter higher cutting loads and forces, resulting in quicker wear. Furthermore, milling mechanics must be considered to better comprehend V_b with various cutting settings and cooling regimes. The main tool wear modes under MQL and flood cooling during the milling of AISi10Mg are shown in Fig. 13. Adhesion, abrasion and chipping are the prominent mechanisms of wear in metal cutting [46]. Under flood and MQL conditions, the coating and chip bonding on the flank face indicated that the tool had undergone a dynamic adhesion-delamination during the cutting process. The hard Si particles in the workpiece are forced against the tool

Fig. 8 SEM and 3D roughness images of AISi10Mg under distinct environments

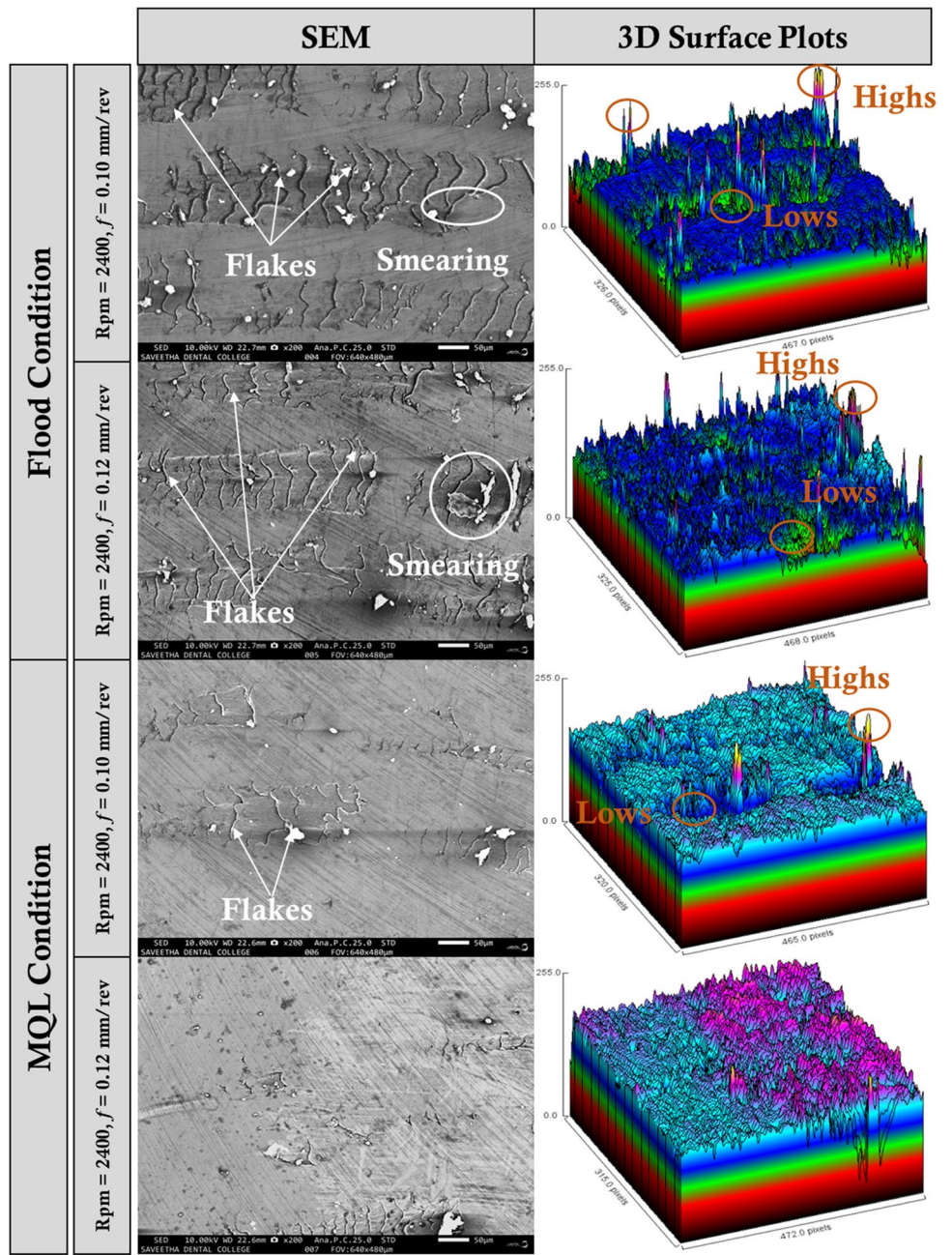


Fig. 9 Influence of cooling strategies on milling temperature under distinct environments **a** $f=0.10$ mm/rev and **b** $f=0.12$ mm/rev

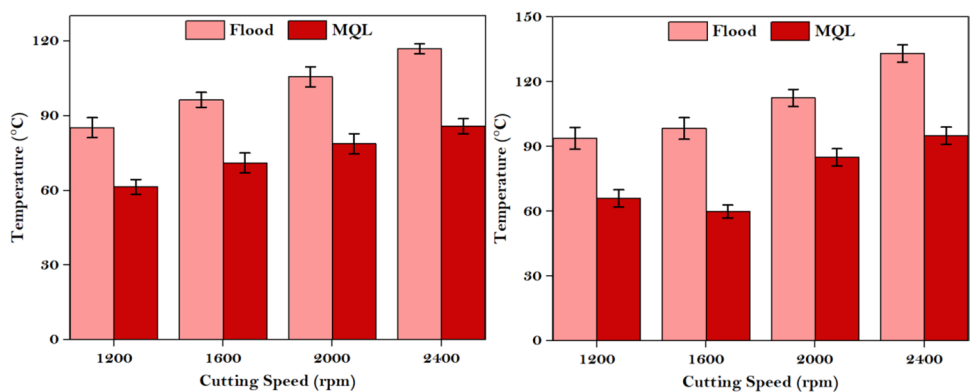


Fig. 10 Main effects plot for milling temperature

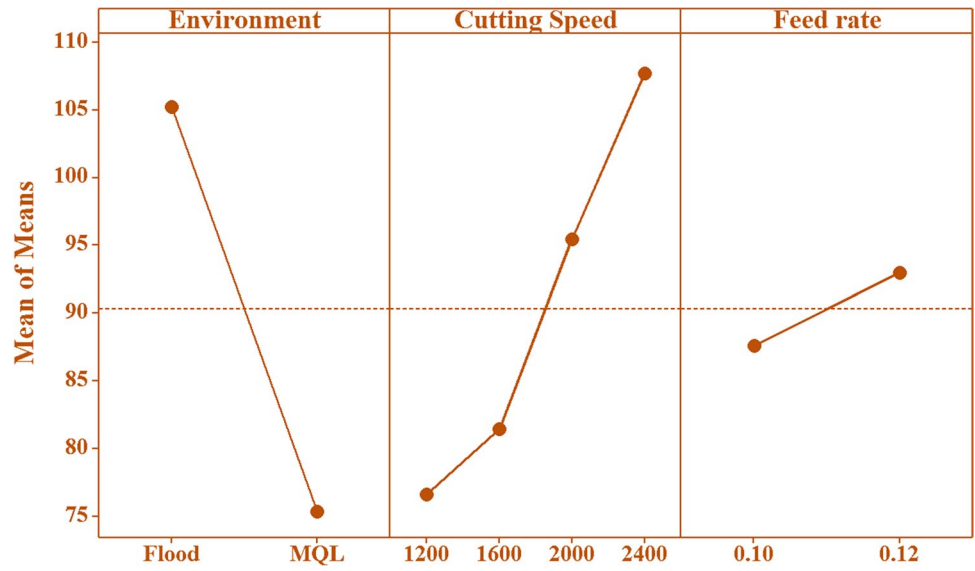


Fig. 11 Influence of cooling strategies on flank wear under distinct environments **a** $f=0.10$ mm/rev and **b** $f=0.12$ mm/rev

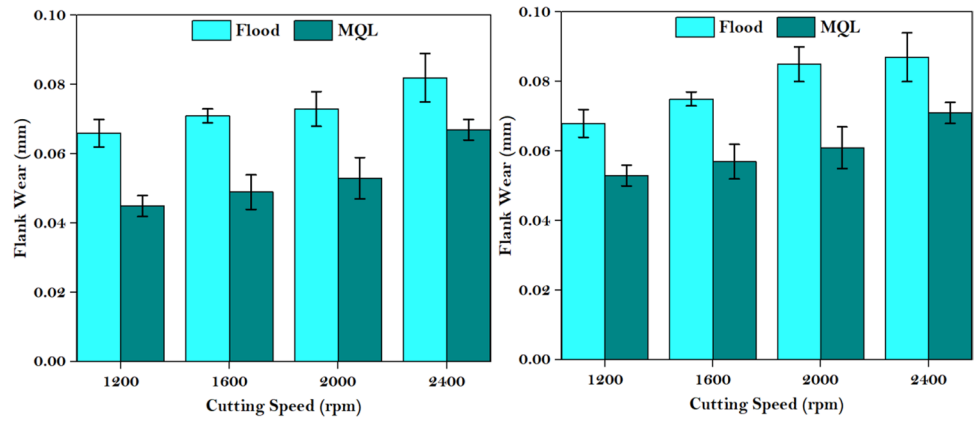


Fig. 12 Main effects plot for flank wear

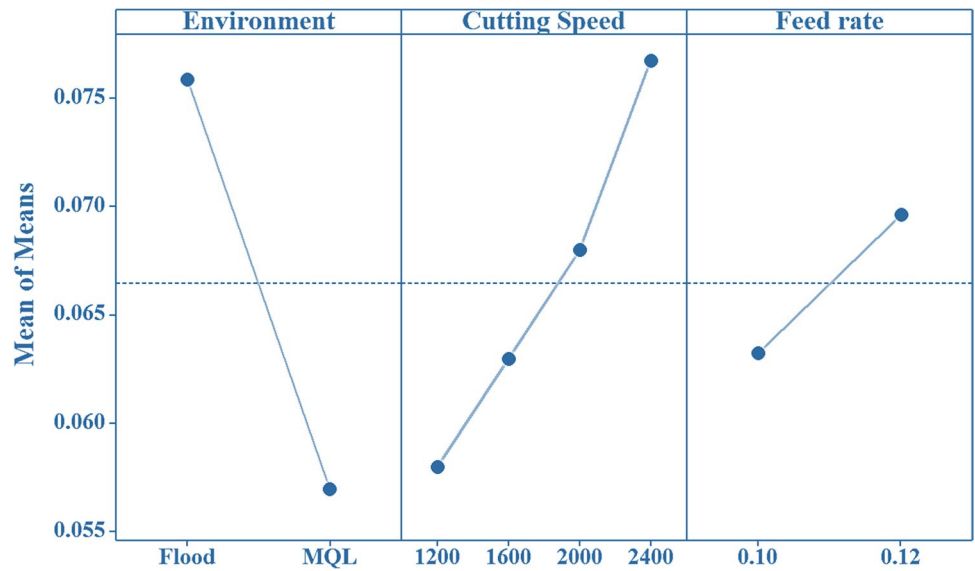
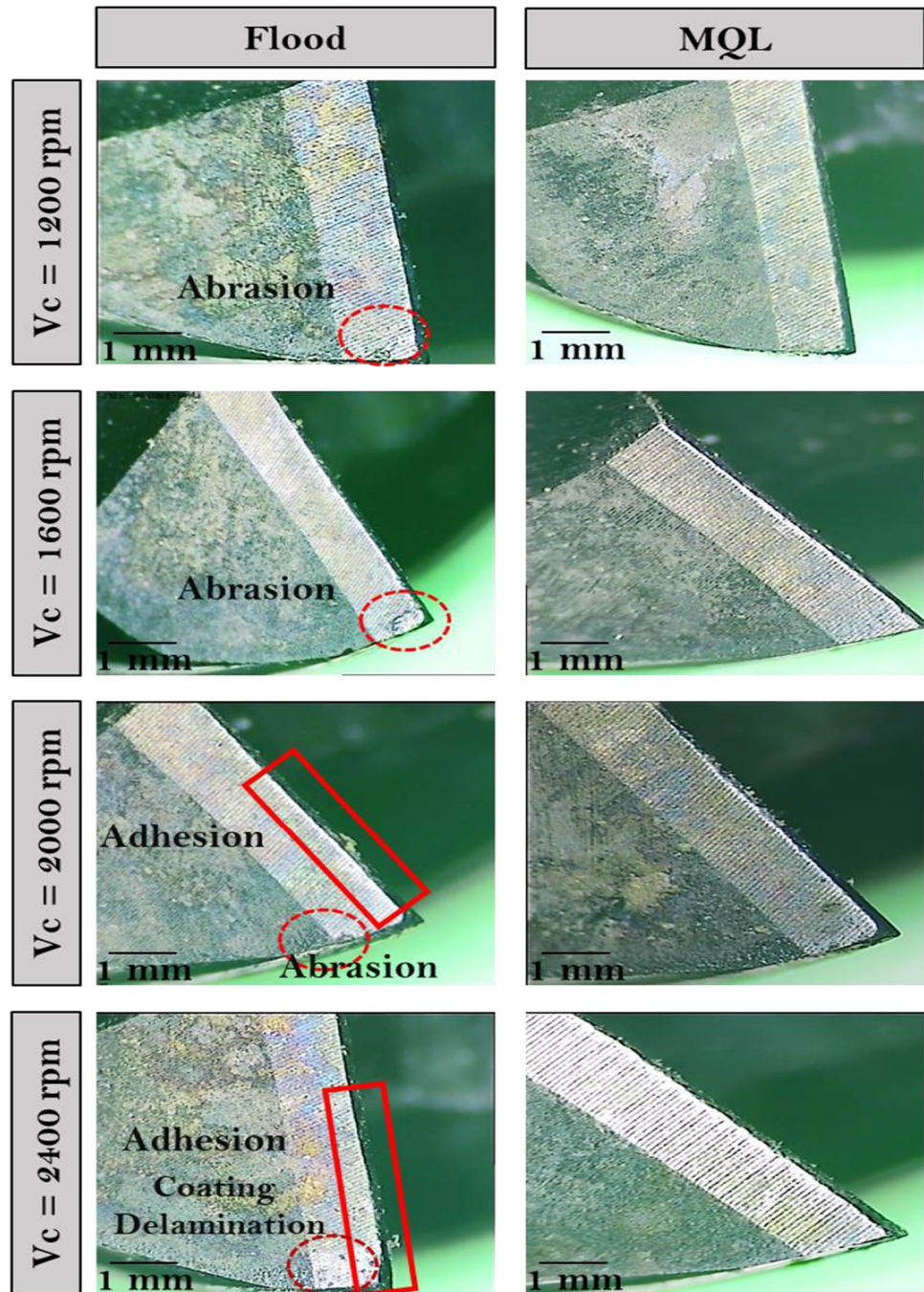


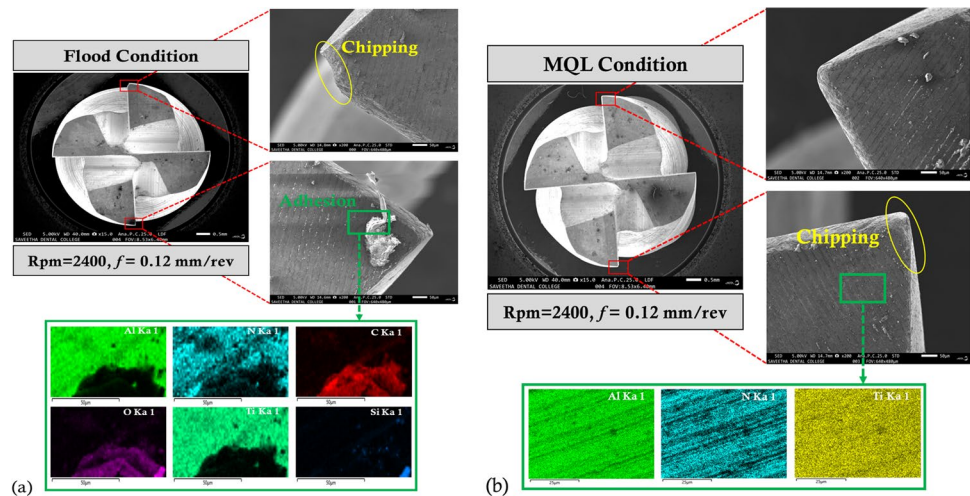
Fig. 13 VRD images of coated tool under distinct environments



surfaces, causing abrasive wear. During the processes of chip formation, the chip slides rapidly on the rake face, generating excessive contact friction and cutting temperature at the tool-chip interface. Under MQL, the oil film can maintain its lubrication ability for a longer period to decrease friction that further lowers the C_T , which was studied in his research by Ross et al. [28]. As a result, longer tool life and better processing quality can be achieved. Flood cooling inherently causes chip adhesion, resulting even in the

delamination of coating at an elevated speed. The results suggested that ensuring a high lubrication environment is more beneficial for extending the tool life than reducing the heat generation. Figure 14a and b shows the SEM and EDS images of the tool under flood and MQL environment. Adhesion and chipping were seen when milling with flood condition. The EDS mapping shows the adhesion of the Si element in the cutter. Less amount of chipping is seen with the MQL strategy as a reason for the high lubrication effect

Fig. 14 SEM and EDS images of coated tool under **a** flood environment and **b** MQL environment



by the oil droplets. The EDS mapping with MQL environment displayed no adhesion of work material on the surface of the cutter.

3.2.4 Microstructural surface deformation

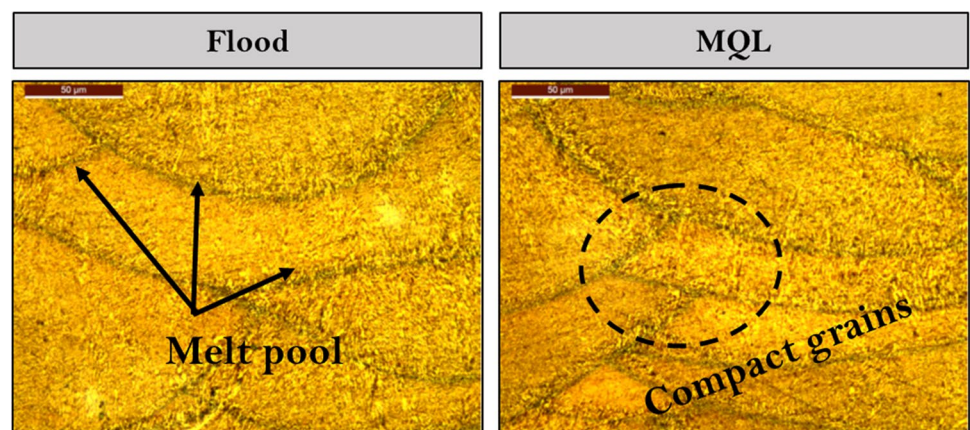
Quality assurance has always been important in production, both ancient and modern. Surface integrity, as defined by the industrial community, refers to the entire assemblage of the surface structure, encompassing physical, mechanical, metallurgical and biological states. Plastic deformation, microcracks, phase transformation, microhardness, recrystallization and residual stress are all reasons for microstructure alteration [46]. The produced heat at the cutter-workpiece contact is crucial to the evolution of microstructure in machining. The microstructure of AlSi10Mg machined with disparate cutting strategies at a V_c of 2400 rpm and a f of 1.2 mm/rev is presented in Fig. 15. The rate of cooling is slow during flood condition. As a result of the heat produced during machining, the

recrystallized grains under the machined face suffer grain growth. By using flood coolant, only the grains near to the surface will be cooled. As a result, with flood cooling, larger grains are found. The quick heating when milling and cooling with MQL reduces the size of the grains on the surface, as shown in the image. In comparison to the flood environment, the MQL condition effectively lowers friction, which lessens the created heat [47]. However, in comparison to flood conditions, MQL creates even more compact grains.

4 Statistical analysis using ANOVA

ANOVA is a tool (statistical) engaged to recognise the consequence of the variables related to outcomes established on the investigational data [15]. In ANOVA, the P -value represents the statistical significance of a confidence interval of 95% (i.e., significance level $\alpha=0.05$); if the P -value is lower than α , then that factor (or source) is significant.

Fig. 15 Microstructural impact under varied colling at a $V_c=2400$ rpm and $f=1.2$ mm/rev



Tables 2, 3 and 4 displayed the ANOVA for Ra, C_T and Vb. The effect of various parameters on the machinability study is displayed in Fig. 16. The environment shows the utmost significance with a contribution of 59.46%, 56.41% and 58% for Ra, C_T and Vb, respectively. The f showed the lowest contribution of 5.79%, 1.83% and 8%, and the V_c showed the middle range contribution of 33%, 36% and 33% for Ra, C_T and Vb, respectively. From the previous examines, it was strong that environmental conditions occupy a bigger role in the part quality and longer life of the machined product.

It is clear that the models considered for Ra, C_T and Vb are adequate and can precisely forecast the o/p parameters in the choice of cutting conditions employed. The linear model is employed to evaluate the effects of i/p parameters and their connections with o/p responses. The regression equations are obtained for the output parameters represented by Ra, C_T and Vb in Eqs. (1,2), (3,4) and (5,6) respectively. Figure 17 illustrates the variation amongst predicted and experimental values of Ra, C_T and Vb. The R^2 value noted for Ra is 0.98, C_T is 0.94 and

Vb is 0.96. The divergence of predicted was smaller in assessment with experimental values.

Selected process parameters have different degrees of effect on responses. A general investigation has been performed on the influence of input factors on each response before doing optimization. Figure 18 shows the contour plots for Ra, C_T and Vb for distinct environmental conditions. From the figure, one can see lower V_c with higher f in flood cutting generates larger Ra in relation to MQL, which is undesirable. Thermal softening of the workpiece at higher V_c indirectly helps to lessen Ra and lower f crops less roughness because of fewer scratches on the machined surface. But at f , productivity is somewhat compromised. In that case, it is very crucial to find out the optimal condition of milling with less compromise of productivity and better surface quality.

Higher speed rises the C_T for both the cutting environments that are visible in the contours of temperature. Moreover, lower speed has a positive impact on C_T ; so, an optimal setting for achieving lower temperature is needed, which has a direct influence on Ra and cutter wear.

Table 2 ANOVA for Ra

Source	Sum of squares	DF	Mean square	F-value	P-value	
Model	0.4897	3	0.1632	199.01	<0.0001	Significant
A-cutting speed	0.1638	1	0.1638	199.69	<0.0001	
B-feed rate	0.0289	1	0.0289	35.23	<0.0001	
C-environment	0.2970	1	0.2970	362.09	<0.0001	
Residual	0.0098	12	0.0008			
Cor Total	0.4996	15				

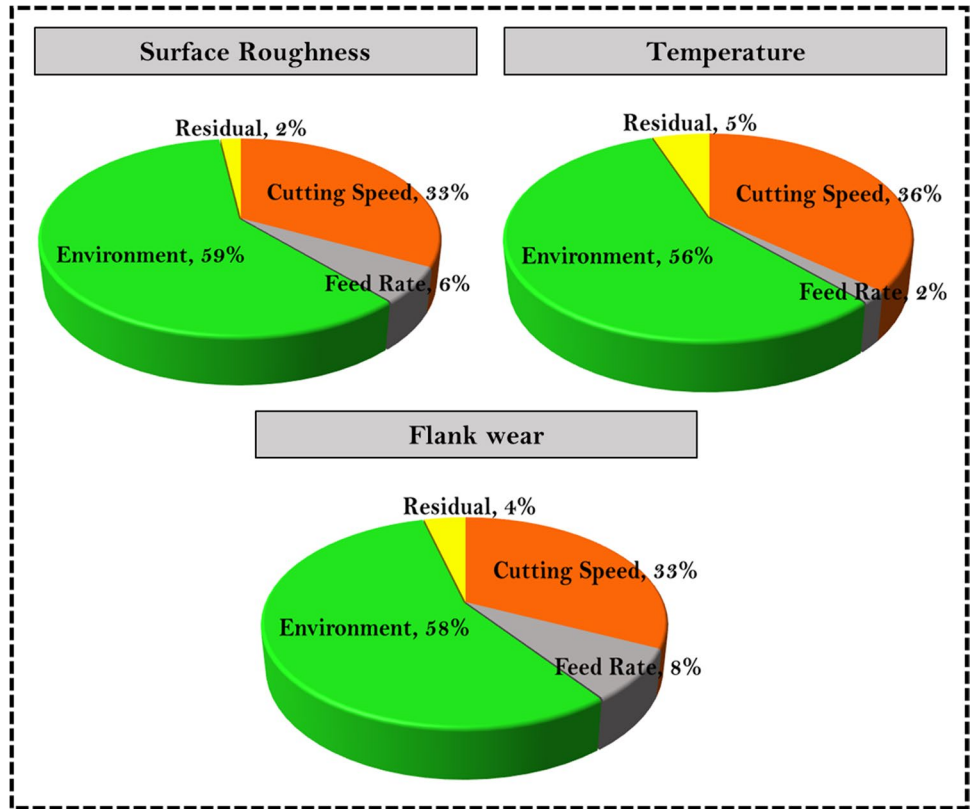
Table 3 ANOVA for C_T

Source	Sum of squares	DF	Mean square	F-value	P-value	
Model	5985.84	3	1995.28	69.93	<0.0001	Significant
A-cutting speed	2300.51	1	2300.51	80.63	<0.0001	
B-feed rate	115.56	1	115.56	4.05	0.0672	
C-environment	3569.76	1	3569.76	125.12	<0.0001	
Residual	342.37	12	28.53			
Cor Total	6328.21	15				

Table 4 ANOVA for Vb

Source	Sum of squares	DF	Mean square	F-value	P-value	
Model	0.0023	3	0.0008	123.05	<0.0001	Significant
A-cutting speed	0.0008	1	0.0008	118.47	<0.0001	
B-feed rate	0.0002	1	0.0002	25.67	0.0003	
C-environment	0.0014	1	0.0014	225.01	<0.0001	
Residual	0.0001	12	6.333E-06			
Cor Total	0.0024	15				

Fig. 16 Effect of various parameters on the responses of machinability study

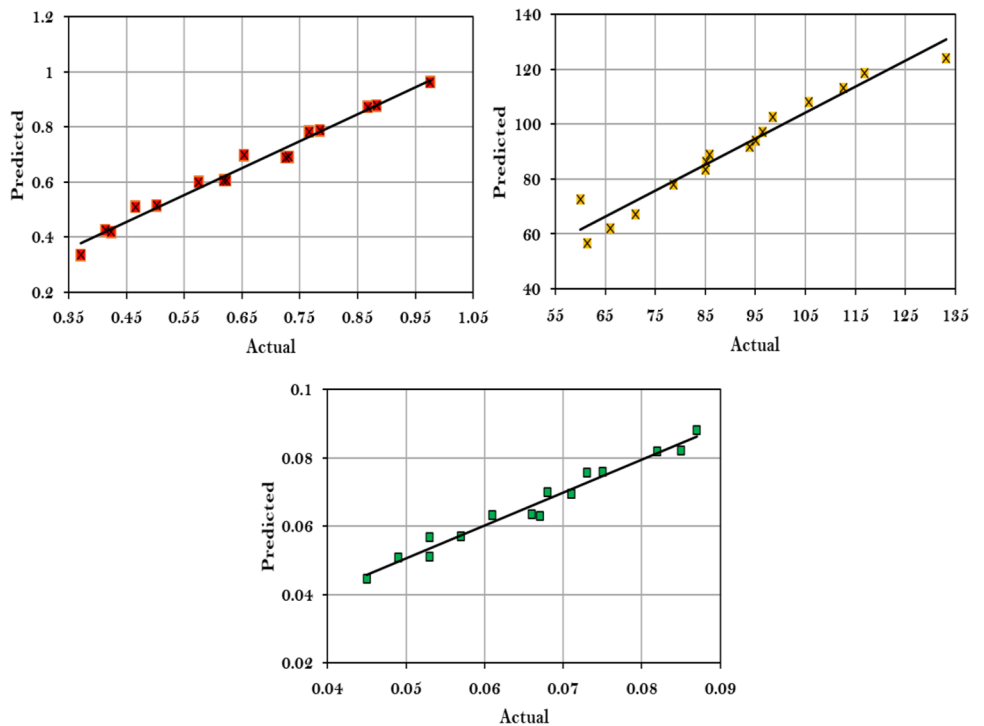


From the contour plot of V_b , it is noted that minimum wear was found at a lower speed-feed combo, which is similar for both the cutting environments. For sustainable manufacturing, optimal settings are required to reduce the cutter wear.

$$Ra - Flood = +0.724750 - 0.000226 \times CuttingSpeed + 4.25000 \times FeedRate \tag{1}$$

$$Ra - MQL = +0.452250 - 0.000226 \times CuttingSpeed + 4.25000 \times FeedRate \tag{2}$$

Fig. 17 Assessment of experimental and predicted values. **a** Surface roughness, **b** milling temperature and **c** flank wear



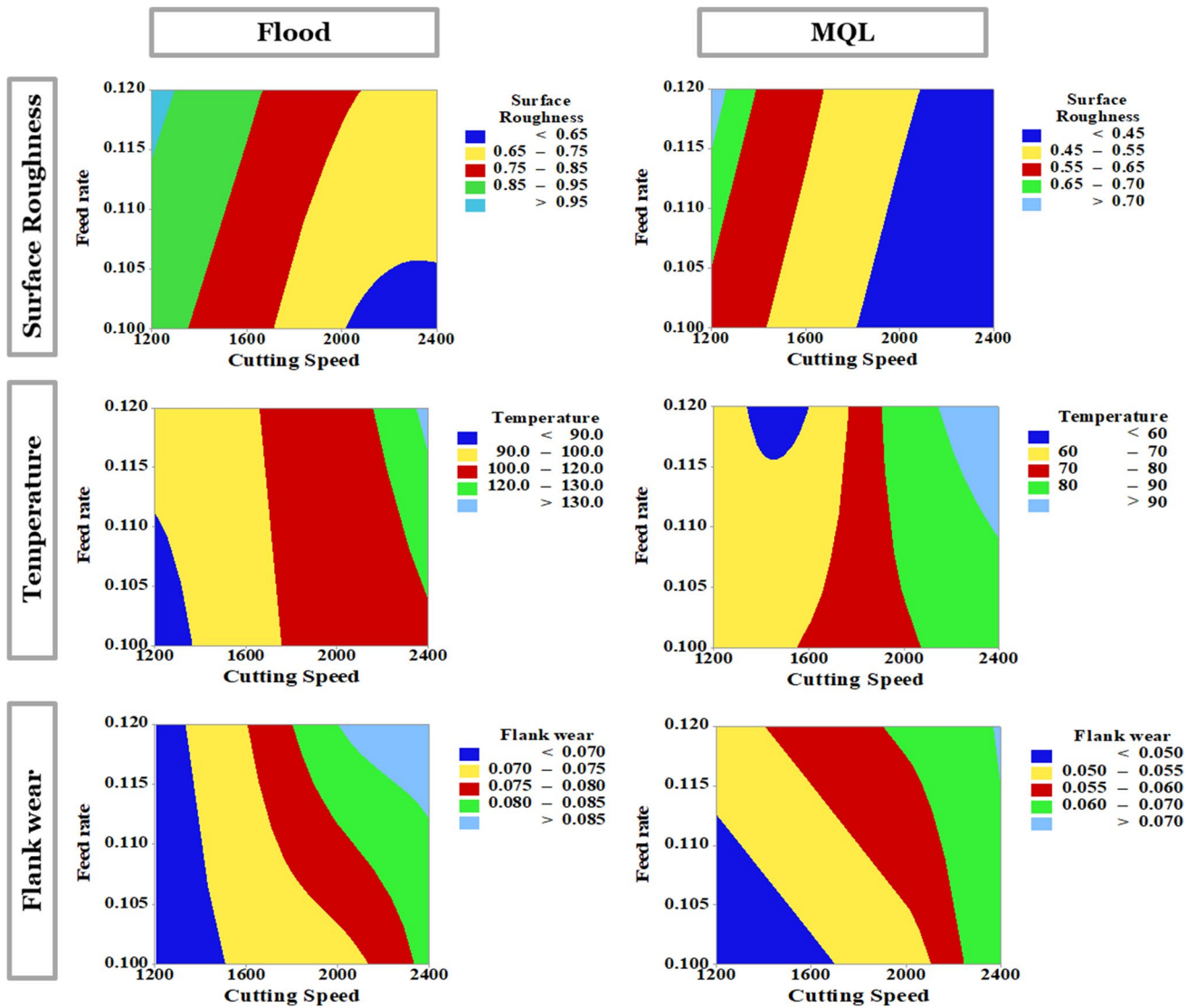


Fig. 18 Contour plots of surface roughness, temperature and flank wear with varied speed-feed combo and cutting environments

$$C_T - Flood = +27.425 - 0.0268125 \times CuttingSpeed - 268.75 \times FeedRate \tag{3}$$

$$C_T - MQL = -2.4487500 - 0.0268125 \times CuttingSpeed - 268.75 \times FeedRate \tag{4}$$

$$V_b - Flood = +0.013250 + 0.000015 \times CuttingSpeed + 0.318750 \times FeedRate \tag{5}$$

$$V_b - MQL = -0.005625 + 0.000015 \times CuttingSpeed + 0.318750 \times FeedRate \tag{6}$$

5 Optimization of responses

The desirability function (DF) was created to optimise the metal cutting process for multiple uses. The procedures are designed to reduce the number of trials required. It transforms a multi-response into a single output. The DF’s ultimate goal is to find the optimal combination of cutting parameters.

$$D = [d_1(Y_1).d_2(Y_2)...d_k(Y_k)]^{1/k} \tag{7}$$

k is number of responses; $d_i(Y_i) = 0$, then it is completely undesirable; $d_i(Y_i) = 1$, then it is highly desirable.

For this milling investigation, DF based on RSM (Fig. 19) is employed to predict the most ideal milling parameters (f , V_c and E) while cutting AM- AlSi10Mg with PVD-coated end mill. For this optimization case, all the responses and input parameters have been given equal importance. The best condition observed was $E = \text{MQL}$, $V_c = 1326.37$ rpm and $f = 0.1$ mm/rev. The responses produced by the best condition was roughness = 0.557 μm , temperature = 59.99 $^\circ\text{C}$ and flank wear = 0.04465 mm, with a top DF value of 0.91. The received outcome is advantageous for manufacturers and offers extreme tool life and the finest surface trait by dropping the environmental effects.

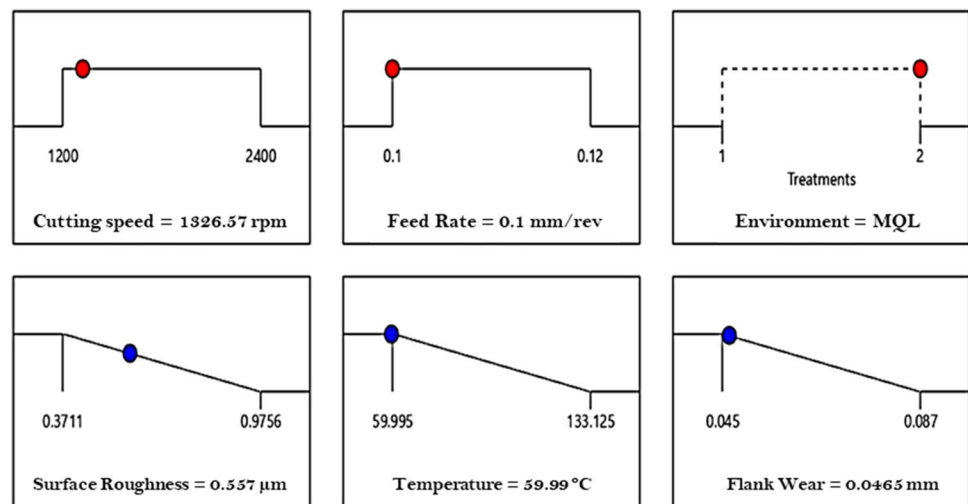
6 Conclusions

The mechanical performance and machinability of 90° oriented AlSi10Mg parts were investigated in this study in accordance with the direction of cutter feed motion and the BUD of the workpiece with distinct speed-feed pairing and cutting environments (flood and MQL with VO).

- 90° oriented AlSi10Mg parts show maximum tensile strength and yield strength of 418 MPa and 234 MPa due to the occurrence of strong bonding along the Z-direction which attributes to the lower elongation percentage of 5.46%, and also the maximum hardness of 107 HBW was evident in the fabricated 90° oriented AlSi10Mg parts. The presence of eutectic Si particles possesses a significant role in improving the wear resistance of the 90° oriented AlSi10Mg parts which was revealed in the worn-out surface of the wear specimen using SEM.

- Under the MQL method, a machined face provides a fine surface characteristic concerning the flood environment. The decrease in roughness is due to the high lubricating action of MQL. The use of MQL declines the R_a by about 25–42% with flood cooling. For all cutting circumstances, SEM pictures revealed flake pieces emerging from the surface, which is solely dependent on the fusing contact angle and laser beam thickness. The 3D surface topography shows the alteration of surface profiles under distinct cooling regimes.
- In the MQL method, VO droplets out from the nozzle mitigate the heat generated at the interface between the workpiece and the tool. MQL lessen the C_T by 24–39% in comparison to flood cooling condition. The reduction of friction values was the primary cause of reduced temperature generation.
- MQL creates a thin film layer at the interface between the workpiece and the tool and this minimises the wear of the cutter to a certain extent. The reduction of flank wear was found to be 18–31% under MQL condition. Adhesion was seen in all flood cutting settings as a reason for the workpiece's leaning to bond with the cutter. The performed EDS analysis shows no adhesion of foreign elements on the surface of the cutter when machining with an MQL environment.
- A noteworthy microstructure modification was observed after milling with the MQL environment concerning flood coolant. The reason behind this is due to the application of MQL, and the droplets in contact with the cutter nullify the heat created at that instance and supply the cooling effect.
- ANOVA test was used to determine the effect of independent variables on a dependent variable. The utmost contribution factor was given by the environment. The optimal cutting condition for milling LPBF- AlSi10Mg is $V_c = 1326$ rpm, $f = 0.1$ mm/rev and cutting environment is MQL.

Fig. 19 Ramp plot for optimised process parameters



Declarations

Ethics approval and consent to participate Not applicable.

References

- Maamoun AH, Elbestawi MA, Veldhuis SC (2018) Influence of shot peening on alsi10mg parts fabricated by additive manufacturing. *J Manuf Mater Process* 2:1–16. <https://doi.org/10.3390/jmmp2030040>
- Kayacan MY, Özsoy K, Duman B et al (2019) A study on elimination of failures resulting from layering and internal stresses in powder bed fusion (PBF) additive manufacturing. *Mater Manuf Process* 34:1467–1475. <https://doi.org/10.1080/10426914.2019.1655151>
- Della Gatta R, Del Sol I, Caraviello A, Astarita A (2021) Selective laser melting of an Al-Si-Mg-Cu alloy: feasibility and processing aspects. *Mater Manuf Process* 36:1438–1449. <https://doi.org/10.1080/10426914.2021.1906900>
- Saravanakumar A, Rajeshkumar L, Balaji D, Jithin Karunan MP (2020) Prediction of wear characteristics of AA2219-Gr matrix composites using GRNN and Taguchi-based approach. *Arab J Sci Eng* 45:9549–9557. <https://doi.org/10.1007/s13369-020-04817-8>
- Lee H, Lim CHJ, Low MJ et al (2017) Lasers in additive manufacturing: a review. *Int J Precis Eng Manuf - Green Technol* 4:307–322. <https://doi.org/10.1007/s40684-017-0037-7>
- Kumar MS, Javidrad HR, Shanmugam R et al (2021) Impact of print orientation on morphological and mechanical properties of L-PBF based AlSi7Mg parts for aerospace applications. *SILICON*. <https://doi.org/10.1007/s12633-021-01474-w>
- Shakerin S, Hadadzadeh A, Amirkhiz BS et al (2019) Additive manufacturing of maraging steel-H13 bimetal using laser powder bed fusion technique. *Addit Manuf* 29:100797. <https://doi.org/10.1016/j.addma.2019.100797>
- Koutiri I, Pessard E, Peyre P et al (2018) Influence of SLM process parameters on the surface finish, porosity rate and fatigue behavior of as-built Inconel 625 parts. *J Mater Process Technol* 255:536–546. <https://doi.org/10.1016/j.jmatprotec.2017.12.043>
- Yap CY, Chua CK, Dong ZL et al (2015) Review of selective laser melting: materials and applications. *Appl Phys Rev* 2. <https://doi.org/10.1063/1.4935926>
- Zakay A, Aghion E (2019) Effect of post-heat treatment on the corrosion behavior of AlSi10Mg alloy produced by additive manufacturing. *Jom* 71:1150–1157. <https://doi.org/10.1007/s11837-018-3298-x>
- Li X, Ni J, Zhu Q et al (2017) Structure and mechanical properties of the AlSi10Mg alloy samples manufactured by selective laser melting. *IOP Conf Ser Mater Sci Eng* 269. <https://doi.org/10.1088/1757-899X/269/1/012081>
- Rajesh Kumar L, Saravanakumar A, Bhuvaneshwari V et al (2019) Optimization of wear behaviour for AA2219-MoS2 metal matrix composites in dry and lubricated condition. *Mater Today Proc* 27:2645–2649. <https://doi.org/10.1016/j.matpr.2019.11.087>
- Baitimerov R, Lykov P, Zherebtsov D et al (2018) Influence of powder characteristics on processability of AlSi12 alloy fabricated by selective laser melting. *Materials (Basel)* 11:1–14. <https://doi.org/10.3390/ma11050742>
- Nicoletto G (2020) Influence of rough as-built surfaces on smooth and notched fatigue behavior of L-PBF AlSi10Mg. *Addit Manuf* 34:101251. <https://doi.org/10.1016/j.addma.2020.101251>
- Saravanakumar A, Sivalingam S, Kumar LR (2018) Dry sliding wear of AA2219/Gr metal matrix composites. *Mater Today Proc* 5:8321–8327. <https://doi.org/10.1016/j.matpr.2017.11.524>
- Salmi A, Atzeni E (2020) Residual stress analysis of thin AlSi10Mg parts produced by laser powder bed fusion. *Virtual Phys Prototyp* 15:49–61. <https://doi.org/10.1080/17452759.2019.1650237>
- Letenneur M, Kreitsberg A, Brailovski V (2019) Optimization of laser powder bed fusion processing using a combination of melt pool modeling and design of experiment approaches: density control. *J Manuf Mater Process* 3. <https://doi.org/10.3390/jmmp3010021>
- Tofail SAM, Koumoulos EP, Bandyopadhyay A et al (2018) Additive manufacturing: scientific and technological challenges, market uptake and opportunities. *Mater Today* 21:22–37. <https://doi.org/10.1016/j.mattod.2017.07.001>
- Shanmugam R, Ramoni M, Thangamani G, Thangaraj M (2021) Influence of additive manufactured stainless steel tool electrode on machinability of beta titanium alloy. *Metals (Basel)* 11. <https://doi.org/10.3390/met11050778>
- Nguyen QB, Luu DN, Nai SML et al (2018) The role of powder layer thickness on the quality of SLM printed parts. *Arch Civ Mech Eng* 18:948–955. <https://doi.org/10.1016/j.acme.2018.01.015>
- Nimel Sworna Ross K, Manimaran G (2019) Effect of cryogenic coolant on machinability of difficult-to-machine Ni–Cr alloy using PVD-TiAlN coated WC tool. *J Brazilian Soc Mech Sci Eng* 41:1–14. <https://doi.org/10.1007/s40430-018-1552-3>
- Zhang H, Dang J, Ming W et al (2020) Cutting responses of additive manufactured Ti6Al4V with solid ceramic tool under dry high-speed milling processes. *Ceram Int* 46:14536–14547. <https://doi.org/10.1016/j.ceramint.2020.02.253>
- Zimmermann M, Müller D, Kirsch B et al (2021) Analysis of the machinability when milling AlSi10Mg additively manufactured via laser-based powder bed fusion. *Int J Adv Manuf Technol* 112:989–1005. <https://doi.org/10.1007/s00170-020-06391-7>
- Dabwan A, Anwar S, Al-Samhan AM et al (2021) Investigations on the effect of layers' thickness and orientations in the machining of additively manufactured stainless steel 316L. *Materials (Basel)* 14. <https://doi.org/10.3390/ma14071797>
- Khan HM, Karabulut Y, Kitay O et al (2020) Influence of the post-processing operations on surface integrity of metal components produced by laser powder bed fusion additive manufacturing: a review. *Mach Sci Technol* 25:118–176. <https://doi.org/10.1080/10910344.2020.1855649>
- Nimel Sworna Ross K, Manimaran G, Anwar S et al (2021) Investigation of surface modification and tool wear on milling Nimonic 80A under hybrid lubrication. *Tribol Int* 155:106762. <https://doi.org/10.1016/j.triboint.2020.106762>
- Ross NS, Mia M, Anwar S et al (2021) A hybrid approach of cooling lubrication for sustainable and optimized machining of Ni-based industrial alloy. *J Clean Prod* 321:128987. <https://doi.org/10.1016/j.jclepro.2021.128987>
- Ross NS, Sheeba PT, Jebaraj M, Stephen H (2021) Milling performance assessment of Ti-6Al-4V under CO2 cooling utilizing coated AlCrN/TiAlN insert. *Mater Manuf Process* 00:1–15. <https://doi.org/10.1080/10426914.2021.2001510>
- Kannan C, Ramanujam R, Balan ASS (2018) Machinability studies on Al 7075/BN/Al2O3 squeeze cast hybrid nanocomposite under different machining environments. *Mater Manuf Process* 33:587–595. <https://doi.org/10.1080/10426914.2017.1401718>
- Nimel Sworna Ross K, Manimaran G (2020) Machining investigation of Nimonic - 80A superalloy under cryogenic CO 2 as coolant using PVD - TiAlN / TiN coated tool at 45 ° nozzle angle. *Arab J Sci Eng*. <https://doi.org/10.1007/s13369-020-04728-8>

31. Struzikiewicz G, Sioma A (2020) Evaluation of surface roughness and defect formation after the machining of sintered aluminum alloy AlSi10Mg. *Materials* (Basel) 13. <https://doi.org/10.3390/ma13071662>
32. Saravana Kumar M, Mohan E, Robinson S, Thivya Prasad D (2021) Comparative study on morphological, physical and mechanical characteristics of L-PBF based AlSi10Mg parts with conventional stir casted Al-10 %SiC composites. *SILICON*. <https://doi.org/10.1007/s12633-021-01065-9>
33. Sk M, Rb S, M V, K NSR, (2020) Applying visualization techniques to study the fluid flow pattern and the particle distribution in the casting of metal matrix composites. *J Manuf Process* 58:668–676. <https://doi.org/10.1016/j.jmapro.2020.08.044>
34. Figiel H, Zogał O, Yartys V (2005) Journal of Alloys and Compounds: Preface. *J Alloys Compd* 404–406:1. <https://doi.org/10.1016/j.jallcom.2005.05.002>
35. Shaikh AS, Schulz F, Minet-Lallemand K, Hryha E (2021) Microstructure and mechanical properties of Haynes 282 superalloy produced by laser powder bed fusion. *Mater Today Commun* 26:102038. <https://doi.org/10.1016/j.mtcomm.2021.102038>
36. Kumar MS, Vasumathi M, Begum SR et al (2021) Influence of B4C and industrial waste fly ash reinforcement particles on the micro structural characteristics and mechanical behavior of aluminium (Al–Mg–Si–T6) hybrid metal matrix composite. *J Mater Res Technol* 15:1201–1216. <https://doi.org/10.1016/j.jmrt.2021.08.149>
37. Saravana Kumar M, Begum SR, Vasumathi M (2019) Influence of stir casting parameters on particle distribution in metal matrix composites using stir casting process. *Mater Res Express* 6:1065d4. <https://doi.org/10.1088/2053-1591/ab4045>
38. Saravana Kumar M, Pruncu CI, Harikrishnan P et al (2021) Experimental investigation of in-homogeneity in particle distribution during the processing of metal matrix composites. *SILICON*. <https://doi.org/10.1007/s12633-020-00886-4>
39. Günan F, Kivak T, Yıldırım ÇV, Sarıkaya M (2020) Performance evaluation of MQL with AL 2 O 3 mixed nanofluids prepared at different concentrations in milling of Hastelloy C276 alloy. *J Mater Res Technol* 9:10386–10400. <https://doi.org/10.1016/j.jmrt.2020.07.018>
40. Yıldırım ÇV, Kivak T, Sarıkaya M, Şirin Ş (2020) Evaluation of tool wear, surface roughness/topography and chip morphology when machining of Ni-based alloy 625 under MQL, cryogenic cooling and CryoMQL. *J Mater Res Technol* 9:2079–2092. <https://doi.org/10.1016/j.jmrt.2019.12.069>
41. Sreejith PS (2008) Machining of 6061 aluminium alloy with MQL, dry and flooded lubricant conditions. *Mater Lett* 62:276–278. <https://doi.org/10.1016/j.matlet.2007.05.019>
42. Khan MMA, Mithu MAH, Dhar NR (2009) Effects of minimum quantity lubrication on turning AISI 9310 alloy steel using vegetable oil-based cutting fluid. *J Mater Process Technol* 209:5573–5583. <https://doi.org/10.1016/j.jmatprotec.2009.05.014>
43. Dhar NR, Kamruzzaman M, Ahmed M (2006) Effect of minimum quantity lubrication (MQL) on tool wear and surface roughness in turning AISI-4340 steel. *J Mater Process Technol* 172:299–304. <https://doi.org/10.1016/j.jmatprotec.2005.09.022>
44. Rakesh M, Datta S (2020) Machining of Inconel 718 using coated WC Tool: effects of cutting speed on chip morphology and mechanisms of tool wear. *Arab J Sci Eng* 45:797–816. <https://doi.org/10.1007/s13369-019-04171-4>
45. Gupta MK, Mia M, Jamil M et al (2020) Machinability investigations of hardened steel with biodegradable oil-based MQL spray system. *Int J Adv Manuf Technol* 108:735–748. <https://doi.org/10.1007/s00170-020-05477-6>
46. Królczyk G, Feldshtein E, Dyachkova L et al (2020) On the microstructure, strength, fracture, and tribological properties of iron-based MMCs with addition of mixed carbide nanoparticles. *Materials* (Basel) 13. <https://doi.org/10.3390/ma13132892>
47. Ali SM, Dhar NR, Dey SK (2011) Effect of minimum quantity lubrication (Mql) on cutting performance in turning medium carbon steel by uncoated carbide insert at different speed-feed combinations. *Adv Prod Eng Manag* 6:185–196

Publisher's note Springer Nature remains neutral with regard to jurisdictional claims in published maps and institutional affiliations.